Single-Distance, Phase-only Frequency-Domain NIRS for Vascular Oxygenation and Tissue Metabolism: A Monte Carlo Simulation Study

Muaaz Faiyazuddin[a], Haiyang Tang[a], Yiqing Hu[a], Miles Bartlett[b,c], Michael D. Nelson[b], and Hanli Liu[a,*]

[a] University of Texas at Arlington, Department of Bioengineering, Arlington, TX, USA
[b] University of Texas at Arlington, Department of Kinesiology, Arlington, TX, USA
[c] Current address: Bartlett Sciences LLC, Dallas, Texas

Abstract

Significance: Frequency-domain near-infrared spectroscopy (FD-NIRS) currently enables absolute hemoglobin quantification but requires multi-distance measurements of both amplitude attenuation and phase shifts. Notably, existing FD-NIRS approaches have not demonstrated reliable quantification of differential redox-state concentrations of cytochrome c oxidase (CCO_{redox}), a critical metabolic marker.

Aim: We aimed to develop a novel optimization-based algorithm for single source-detector (S-D), phase-only FD-NIRS that achieves accurate quantifications of hemoglobin parameters (HbO and Hb) and CCO_{redox},

Approach: Our computational framework implemented both forward modeling and inverse reconstruction. For the modeling, we first defined chromophore concentration sets (HbO, Hb, CCOredox), followed by calculations of wavelength-dependent optical properties for 2- or 8-wavelength configurations. Next, time-domain photon propagation was generated via Monte Carlo (MC) simulations, and then FD-NIRS parameters (modulation amplitude, phase) were extracted through Fourier analysis. In the inverse computation, nonlinear optimization with edge-barrier regularization was employed for the recovery of chromophore concentrations. Both the multi-separation method and the single S-D, phase-only algorithm were used to reconstruct chromophore concentrations.

Results: Respective performances evaluated by the two methods were compared through their concentration recovery accuracy. In either the 2- or 8-wavelength configuration, our new algorithm outperformed the conventional method for the S-D separations up to 3 cm for all three chromophores. In particular, CCO_{redox} estimation was improved markedly from a mean relative error of 34.1% with the conventional method to just 5.1% using our algorithm.

Conclusions: These results validate single-separation phase-only FD-NIRS as an accurate method for multi-chromophore quantification (including CCO_{redox}), enabling simpler, cost-effective systems without compromising metabolic imaging capability. The approach achieves <10% error in hemoglobin quantification while eliminating traditional multi-distance requirements.

Keywords: Frequency-domain NIRS, absolute quantifications of chromophore concentrations, redox-state of cytochrome c oxidase.

* Corresponding author: hanli@uta.edu

1 Introduction

Near-Infrared Spectroscopy (NIRS) is a noninvasive optical technique that quantifies tissue chromophores by measuring near-infrared light attenuation through biological tissue. Among various NIRS modalities, frequency-domain NIRS (FD-NIRS) utilizes a radio frequency-modulated light source containing both direct and alternating current (DC and AC) components, generating a photon-density wave that propagates through the measured tissue [1, 2]. FD-NIRS devices measure attenuations in both DC and AC amplitudes along with phase shifts of this photon-density wave. By combining these measurements, FD-NIRS enables determination of absolute tissue optical properties - specifically, the absorption coefficient (μ_a) and reduced scattering coefficient (μ_s') - which in turn permit calculation of absolute chromophore concentrations [1, 2]. Theoretically, accurate measurement of tissue μ_a at multiple wavelengths allows quantification of not only vascular oxyhemoglobin (HbO) and deoxyhemoglobin (Hb) concentrations, but also (though more challenging) the differential redox-state concentration of cytochrome c oxidase (CCO) [3, 4].

A widely used approach for quantifying tissue optical properties in vivo using FD-NIRS is the slope method, which requires measurements at multiple source-detector (S-D) separations [1, 2, 5]. This method is based on FD diffusion theory, which demonstrates that in an infinite or a semi-infinite boundary setting, both: (1) the logarithm of the product of AC (or DC) amplitude and S-D separation (ρ), and (2) the phase delay, exhibit linear correlations with ρ [5]. These linear relationships enable determination of the absorption coefficient (μ_a) and reduced scattering coefficient (μ_s') through simple linear regression of the respective slopes [1, 5]. While computationally straightforward and experimentally validated, the slope method has notable limitations. First, it necessitates multiple spatial channels for different ρ values, increasing both

system complexity and cost. More importantly, although employing multiple S-D separations, the method assumes tissue homogeneity across all measurement locations and therefore cannot provide depth-resolved information.

To address these limitations, alternative FD-NIRS strategies have been developed, such as a single-distance but frequency-sweep approach [6] and a dual-slope method [7, 8]. However, these approaches often require more sophisticated hardware (e.g., frequency-sweep device) or rely on additional modeling development [7, 8]. These constraints limit their generalizability and practical utility for clinical or wearable applications, where simplicity, robustness, and cost-effectiveness are paramount.

In this study, we hypothesized that an optimization-based algorithm could simultaneously estimate chromophore concentrations and tissue scattering parameters using only phase-shift measurements from FD-NIRS at a single S-D separation and modulation frequency. To validate this hypothesis, we employed Monte Carlo (MC) simulations to generate FD-NIRS data with well controlled optical properties and chromophore concentrations, enabling rigorous evaluation of the algorithm's performance across diverse parameter conditions. Given its reliance on phase-only FD-NIRS measurements at a single S-D separation, we termed the algorithm FD_{1SD_phase}. As a purely computational tool for post-processing, FD_{1SD_phase} is compatible with conventional FD-NIRS hardware and measurement geometries, ensuring broad applicability.

Furthermore, we expanded the capabilities of our FD_{1SD_phase} framework beyond conventional hemoglobin quantification using dual-wavelength approaches. By simulating FD-NIRS phase measurements across eight carefully selected NIR wavelengths [9], we demonstrate, as a proof of principle, that FD_{1SD_phase} can estimate the differential redox-state concentration of cytochrome c oxidase (CCO_{redox}), defined as the difference between oxidized and reduced CCO

(CCO_{redox} = oxidized [CCO] - reduced [CCO]). Accordingly, CCO_{redox} serves as a critical marker or characteristic of mitochondrial metabolism [4, 10]. While prior studies have quantified *changes* in CCO_{redox} relative to baseline using broadband continuous-wave NIRS [10, 11] or hybrid methods [12], absolute CCO_{redox} quantification remains rare and technically challenging due to its low concentration in tissues and subtle spectral features. Our Monte Carlo simulations reveal that FD_{1SD_phase}, when applied to FD-NIRS data at these eight optimized wavelengths, enables robust CCO_{redox} estimation, particularly at source-detector separations shorter or equal to 2.5 cm.

Through Monte Carlo simulations, this study validates our hypothesis and demonstrates the feasibility of solving the inverse problem using our approach as a standalone methodology. While experimental demonstrations and broader clinical applications remain important future directions, the key contribution of this work lies in developing a single S-D separation, single modulation-frequency, and phase-only FD-NIRS technique. This innovation represents a significant step toward simpler, more cost-effective FD-NIRS implementations that could enhance its practicality for clinical and wearable applications.

2 Theory

2.1. FD Photon Propagation in Scattering Media

In FD-NIRS, a tissue volume is illuminated with intensity-modulated NIR light, and the detected signal at the surface is characterized by both amplitude attenuation and phase delay. These arise due to the combined effects of absorption and scattering within the tissue, and are described by the diffusion approximation to the radiative transport equation, valid under the conditions of high scattering and low absorption [1, 2].

Several analytical solutions to the FD diffusion equation exist, differing primarily in the boundary conditions imposed. The infinite medium model assumes unbounded geometry, while the semi-infinite model reflects the presence of a tissue–air interface. Among these, the semi-infinite solution with extrapolated boundary conditions accounts for refractive index mismatch and surface reflections, offering a more realistic representation of experimental geometry [3, 5]. As such, it has been widely used in FD-NIRS for modeling light propagation in homogeneous tissue volumes. Specifically, eq. (1) models the phase of the photon-density wave as functions of the tissue's absorption coefficient μ_a, reduced scattering coefficient μ_s', source-detector separation ρ, modulation frequency ω, and the speed of light in the medium v.

$$\Phi^s = \rho \cdot \sqrt{\frac{\mu_a}{2D}} \cdot \sqrt{\left(1 + \left(\frac{\omega}{v\mu_a}\right)^2\right) - 1} - \arctan\left(\frac{\rho \cdot \sqrt{\frac{\mu_a}{2D}} \cdot \sqrt{\left(1+\left(\frac{\omega}{v\mu_a}\right)^2\right)-1}}{1+\rho \cdot \sqrt{\frac{\mu_a}{2D}} \cdot \sqrt{\left(1+\left(\frac{\omega}{v\mu_a}\right)^2\right)+1}}\right) \quad (1)$$

In contrast to the slope method, the approach described in this study leverages single-distance, phase-only measurements of FD-NIRS, obtained across multiple wavelengths, to estimate tissue optical properties through a nonlinear optimization strategy. This modeling framework removes the requirement for spatial hardware complexity and enables spectral resolution of individual chromophores.

2.2. Spectral modeling of tissue optical properties

To enable the recovery of physiological parameters from multispectral FD-NIRS measurements, we define the tissue's optical properties as functions of a small number of wavelength-independent variables, as given below. The absorption coefficient at each wavelength λ is modeled as a linear combination of known extinction coefficients and unknown chromophore concentrations:

$$\mu_a(\lambda) = \sum_i \varepsilon_i(\lambda) \cdot [C_i] + \mu_{a,water}(\lambda) \quad (2)$$

where $\varepsilon_i(\lambda)$ is the molar extinction coefficient of chromophore $i \in \{HbO, Hb, CCO\}$, and $\mu_{a,water}$ accounts for water absorption when applicable. In this study, we do not directly fit $\mu_a(\lambda)$ but rather use them as intermediate variables to reconstruct underlying concentrations.

Similarly, the reduced scattering coefficient is modeled using a power-law dependence on wavelength [13]:

$$\mu_s'(\lambda) = a\left(\frac{\lambda_0}{\lambda}\right)^{-b} \quad (3)$$

where a is the scattering amplitude, b is the scattering power, and λ_0 is a reference wavelength (set to 500 nm in this work).

Eqs. (2) and (3) associate the wavelength-independent parameters $[C_i]$, a, and b, with the full spectral profiles of $\mu_a(\lambda)$ and $\mu_s'(\lambda)$. When multi-wavelength (e.g., > 8) measurements are performed, parameterization given by eqs. (2) and (3) is the key to significantly reduce the dimensionality of the inverse problem. Rather than reconstructing a separate pair of μ_a and μ_s' for each wavelength, this study reconstructed a compact set of physiologically meaningful parameters (i.e., chromophore concentrations and tissue scattering properties), from which the full optical spectra can be also obtained. In this way, we enabled effective spectral unmixing from a limited number of measurements, including configurations with only two wavelengths for obtaining HbO and Hb or eight wavelengths for estimating HbO, Hb, and CCO_{redox}.

2.3. Inverse estimation with nonlinear optimization

The estimation of tissue physiological parameters is considered as a nonlinear inverse problem. Given multi-wavelength phase measurements at a fixed S-D separation and modulation frequency, the goal of this study was to recover the underlying chromophore concentrations and scattering parameters that minimize the discrepancy between the measured and predicted phase shifts.

Given the analytical phase expression described in eq. (1) and the spectral parameterizations defined by eqs. (2) ad (3), the inverse problem is then formulated as the minimization of a cost function, defined as the sum of squared errors between the modeled and simulated phase values across all the wavelengths selected, as shown by eq. (4):

$$Error = \sum_{\lambda}[\varphi_{model}(\lambda;\theta) - \varphi_{meas}(\lambda)]^2 + R(\theta) \quad (4)$$

where, $\varphi_{model}(\lambda;\theta)$ denotes the predicted phase at wavelength λ, computed from the model using the parameter set $\theta = \{[HbO], [Hb], [CCOredox],\ a,\ b\}$. The $\varphi_{meas}(\lambda)$ represents the phase shift values obtained from Monte Carlo simulations. The first term in cost function, eq. (4), captures the spectral mismatch between the model and data, while the second term $R(\theta)$ serves as a regularization penalty.

To enforce physiological plausibility and prevent overfitting, a custom edge-barrier regularization scheme is employed. This penalty discourages parameter values from drifting toward the extremes of their admissible range but remains permissive if the data strongly support such values. Although conceptually related to quadratic penalty methods and soft constraint enforcement in constrained optimization, this formulation was specifically developed for concentrations estimation in this study. The regularization function is defined as:

$$R(\theta_j) = \alpha \cdot \left(\frac{\theta_j - c}{h}\right)^2, \quad where\ c = \frac{lower+upper}{2},\ h = \frac{upper-lower}{2} \quad (5)$$

Each parameter is assigned a penalty weight α, allowing differential control over the smoothness and range tightness of the solution. This formulation favors estimates that lie within physiologically relevant bounds while still allowing deviation if justified by the measured data.

Although FD-NIRS systems typically measure both amplitude and phase of the photon-density wave, this study utilizes only the phase component for inverse estimation. The decision is

based on both theoretical considerations and empirical evaluation. Amplitude measurements in FD systems are strongly influenced by several system-specific scaling factors, including light source intensity, detector sensitivity, light-tissue coupling efficiency, and boundary-related losses. These multiplicative terms introduce ambiguity in amplitude interpretation. To address this, we incorporated an explicit scaling factor β as an additional parameter to be estimated during optimization. This provided flexibility to account for amplitude scaling effects without requiring system calibration or hardware-specific modeling.

To assess the value of amplitude data in practice, we implemented a two-stage optimization strategy in which initial estimates were obtained using phase-only fitting, followed by a joint refinement using both phase and amplitude. However, across multiple simulations, this combined approach yielded only marginal improvements in reconstruction accuracy, while increasing model complexity and introducing additional fitting instability. Based on these findings, phase-only modeling for reconstruction was selected as the final estimation strategy because of its robustness, reduced reliance on calibration, and consistency with the single-distance design.

The cost function (i.e., eq.(4)) was minimized using the L-BFGS-B algorithm, a quasi-Newton method suitable for bounded nonlinear optimization [14]. Parameter bounds were derived from literature-reported physiological ranges [3, 13]. Optimization was performed independently for each measurement point using vectorized spectral fitting, supporting both dual-wavelength and eight-wavelength configurations. Notably, our algorithm demonstrates consistent convergence even when initialized with fixed values that deviate substantially from the ground truth, underscoring its robustness and generalizability.

3. Methods

Figure 1 presents a flowchart summarizing the computer simulation and data analysis workflow. The process begins with a predefined set of chromophore concentrations (HbO and Hb), from which the corresponding $\mu_a(\lambda)$ and $\mu_s'(\lambda)$ spectra are derived. These spectra serve as inputs for time-domain Monte Carlo (MC) simulations. The simulated time-resolved data are then Fourier-transformed to extract FD NIRS parameters, namely, the DC amplitude, AC amplitude, and phase values. Using these FD-NIRS parameters, we applied two distinct reconstruction approaches: One is the conventional slope method (requiring multiple source-detector separations), and our proposed single S-D, phase-only optimization method. The entire workflow was repeated 30 times to simulate 30 independent tissue samples, which can mimic 30 distinct human subjects in a virtual cohort study.

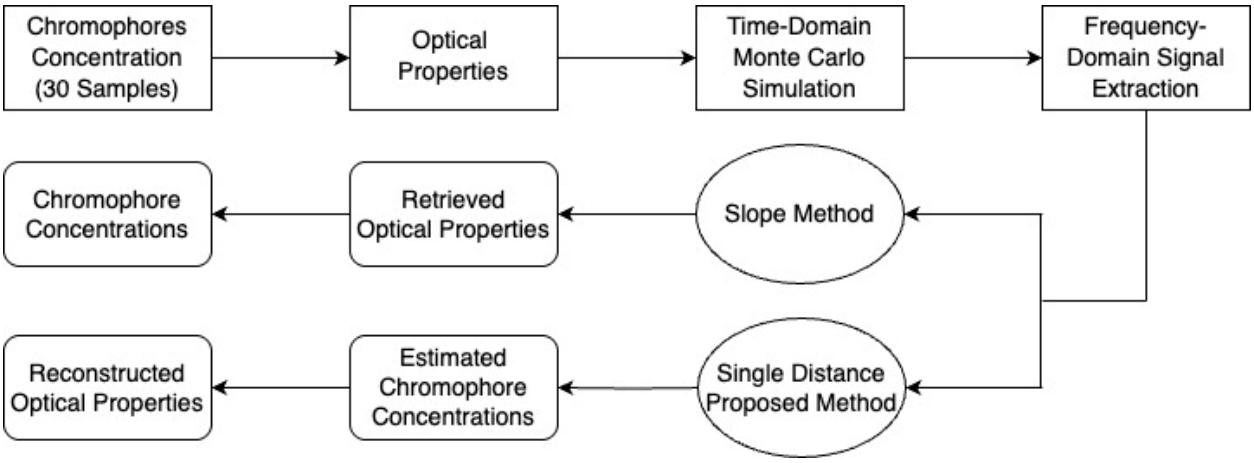

Fig. 1 Flowchart to present the simulation and analysis workflow used in this study. It starts from a chosen set of chromophore concentrations (HbO and Hb with or without CCO_{redox}), followed by corresponding $\mu_a(\lambda)$ for given wavelengths (either 2 or 8 wavelengths). Then, FD-NIRS parameters (i.e., DC, AC, and phase values) were extracted from the time-domain MC simulations after the Fourier transform. Next, both the slope method and single S-D, phase-only optimization method were used to reconstruct chromophore concentrations.

3.1 Synthetic optical property Generation

To evaluate the accuracy and generalizability of the proposed FD_{1SD_phase} inversion framework, we generated controlled synthetic datasets that mimic realistic physiological variability in tissue optical properties. The $\mu_a(\lambda)$ value was computed based on representative concentrations of the dominant NIR chromophores: HbO, Hb, CCO_{redox}. For each of these constituents, a physiological mean concentration was assumed, namely, 60, 25, and 8.5 μM for HbO, Hb, and CCO_{redox}, respectively. Sample-to-sample variation (simulating subject-to-subject) was introduced using random perturbations drawn from a Gaussian distribution with a standard deviation of 10% of the mean. This process was used to generate 30 distinct chromophore profiles, intended to simulate inter-subject or inter-region variability within biological tissues.

Absorption due to water was also included as a background term, scaled by a fixed volume fraction of 75%. For each sample, the total absorption coefficient spectrum was calculated at the selected wavelengths by applying Beer's law across the perturbed concentration vectors. Reduced scattering coefficients $\mu_s'(\lambda)$ were modeled using eq. (3), with base parameters $a = 24.2$ and $b = 1.611$, and a reference wavelength of 500 nm. In analogy to chromophore concentration, the scattering parameters were independently perturbed by 1% across samples to represent subject or anatomical variability in tissue microstructure. This process ensured that both μ_a and μ_s' values were unique for each sample, forming a physiologically diverse basis for forward simulation.

First, two wavelength configurations were used in the study. For hemoglobin-only estimation, MC simulations were performed at 690 nm and 830 nm, which are commonly employed for quantifying HbO and Hb due to their differential absorption profiles. Second, for CCO_{redox} quantification, an eight-wavelength set was adopted (784, 800, 818, 835, 851, 868, 881, and 894 nm) based on a continuous-wave study [9]. This spectral configuration has been previously shown

to enhance sensitivity to the broad and low-concentration absorption features of CCO_{redox} while maintaining discrimination from overlapping hemoglobin signals.

3.2 Monte Carlo simulation and FD signal construction

Time-domain photon propagation was simulated using the $pmcx$ Monte Carlo engine under homogeneous tissue geometry [15]. A cuboidal tissue volume (10 cm per side) was modeled for the Monte Carlo simulations, with an isotropic point source positioned at the center of the top surface and detectors placed at radial distances of 2.0, 2.5, 3.0, and 3.5 cm from the source. Each simulation used sample-specific (i.e., subject-specific) $\mu_a(\lambda)$ and $\mu_s'(\lambda)$ profiles. A fixed anisotropy factor (g) of 0.85 and a refractive index (n) of 1.37 were used for all simulations. For each wavelength and sample, simulations were run with 1.2×10^8 photons and a temporal resolution of 10 ps over a 10 ns acquisition window. This yielded time-resolved photon reflectance waveforms for each detector separation and wavelength combination.

FD measurements were derived by applying a discrete Fourier transform to each reflectance at a modulation frequency of 110 MHz. From the complex FFT output, three quantities were extracted: the DC and AC amplitudes (steady and modulated component of optical fluence) and the phase shift (angular delay). These values were assembled into structured matrices, with each row representing a sample and each column corresponding to a wavelength–separation pair. The resulting dataset simulates realistic FD-NIRS measurements and supports both dual-wavelength and multispectral analysis workflows.

3.3 Slope method for optical property estimation

To provide a reference for evaluating the proposed single-separation, phase-only inversion algorithm, the conventional slope method was applied to the frequency-domain synthetic data. For each wavelength, a linear fit was performed using the phase values and $\ln(\rho^2 \cdot U_{AC})$ against S-D

separation, ρ. The slopes from these two fits were used to compute respective μ_a and μ_s' via standard diffusion theory relations [3, 5]. Once each μ_a value was estimated for each wavelength, chromophore concentrations (i.e., HbO, Hb, with or without CCO_{redox}) recovered via the inversion of the Beer-Lambert law and the known extinction coefficient matrix. This method was applied consistently to both the two-wavelength and eight-wavelength datasets.

3.4 Single-distance, phase-only FD-NIRS optimization algorithm

The proposed inversion framework was developed to estimate tissue chromophore concentrations and scattering parameters exclusively from single-distance, phase-only FD-NIRS measurements. For each synthetic dataset, the algorithm was applied independently to phase data from four distinct S-D separations (2.0, 2.5, 3.0, and 3.5 cm, labeled SD1–SD4), yielding four independent parameter estimations per sample (or simulated subject).

In each MC simulation, for the two-wavelength case, the estimated model parameters included (1) HbO, (2) Hb, (3) wavelength-independent scattering parameters, a and b. When additional CCO_{redox} concentration needs to be determined, the eight-wavelength configuration was used in the optimization process. These four (or five) parameters were optimized via nonlinear least-squares fitting. Subsequently, the spectral profiles of $\mu_a(\lambda)$ and $\mu_s'(\lambda)$ were reconstructed using the relationships given in Eqs. 2 and 3.

We also evaluated a two-feature (i.e., AC amplitude + phase) optimization approach, extending the phase-only fitting process with a gain-scaling parameter. Comparative analyses showed minimal gains in accuracy from including AC amplitude, which is expected given the two-feature method's increased vulnerability to initialization errors and local minima, particularly for single-distance fitting conditions. Thus, the phase-only method's robustness justifies its adoption

for single-distance applications. Accordingly, we present the results obtained with phase-only optimization in the Results section.

3.5 Evaluation metrics and comparison strategy

For either the slope method or our FD_{1SD_phase} algorithm, the estimated chromophore concentrations were compared directly against the known values used during the initial synthetic data generation, which serves as the ground truth values. All estimations were performed or calculated using fixed initial parameter values (e.g., HbO and Hb) and uniform optimization settings across samples, without any re-tuning or sample-specific initialization. This consistent configuration in both methods underscores the generalizability of the proposed algorithm across physiologically variable conditions.

Estimation accuracy was assessed using two complementary metrics. The mean absolute error (MAE) was used to quantify the average magnitude of deviation between estimated and ground-truth values, expressed in physical units (micromolar for concentrations and inverse centimeter for optical coefficients). In parallel, the mean relative error (MRE) was computed by normalizing the absolute deviation by the corresponding ground truth value, providing a scale-invariant measure of performance. These metrics were computed independently for each chromophore species, as well as for μ_a and μ_s' values at each wavelength.

For our FD_{1SD_phase} strategy, each of the four source-detector separations (SD1 through SD4) was treated as an independent estimation path, allowing us to examine the sensitivity of the algorithm's performance to spatial sampling. Results obtained from the single-distance method were then compared to those from the slope method, both of which were evaluated on the same dataset under identical simulation and modeling conditions. This evaluation framework enabled a

direct and comprehensive comparison of estimation fidelity across methods, parameters, and wavelength configurations.

4 Results

4.1 Hemoglobin quantification using two-wavelength configuration

The two-wavelength configuration at 690 nm and 830 nm was used to assess the accuracy of hemoglobin concentration estimates obtained via the proposed FD_{1SD_phase} method. Estimations were performed independently at each of the four S-D separations (2.0, 2.5, 3.0, and 3.5 cm) and were compared against results from the conventional slope method, which used paired AC amplitude and phase measurements across all separations.

Figure 2 compares the estimated versus true concentrations of HbO and Hb across all 30 synthetic samples (representing 30 human subjects). For the Monte Carlo simulations, these synthetic samples were generated with mean concentrations of 60 μM (HbO) and 25 μM (Hb), each perturbed with zero-mean Gaussian noise with a standard deviation equal to 10% of the respective mean concentration to simulate physiological variability. Specifically, Fig. 2(a) displays outcomes from the conventional slope method, while Figs. 2(b)-2(e) show the four single-distance variants (SD1-SD4). Visual inspection reveals strong agreement between reconstructed and true concentrations for both chromophores across all samples. However, estimates obtained at the largest source-detector separation (3.5 cm, SD4) exhibit greater fluctuation and systematic bias (particularly for Hb), suggesting reduced measurement reliability at extended distances.

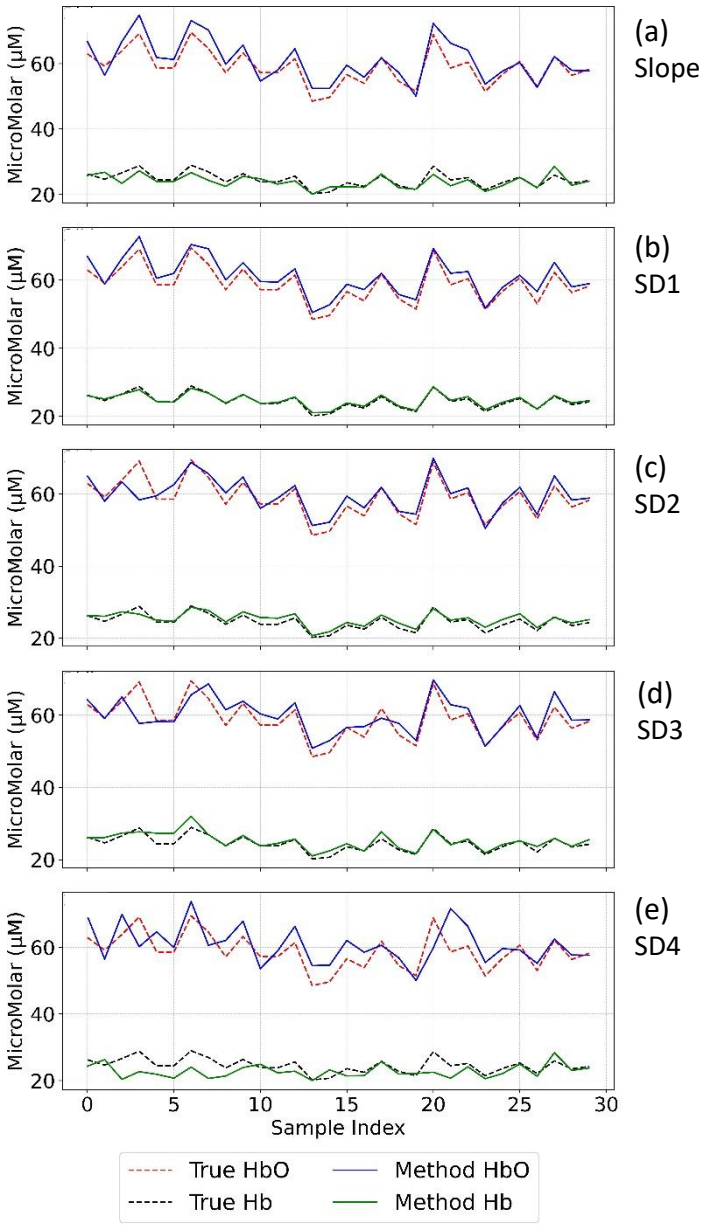

Fig. 2. Comparison of true and estimated concentrations of HbO and Hb across 30 synthetic samples using a two-wavelength FD-NIRS configuration (690 nm and 830 nm). The reconstructed results were obtained using (a) the conventional slope method and FD_{1SD_phase} at (b) SD1 = 2.0 cm, (c) SD2 = 2.5 cm, (d) SD3 = 3.0 cm, and (e) SD4 = 3.5 cm, respectively. Dashed lines represent ground-truth concentrations, while solid lines denote model estimates. The agreement across samples highlights the performance of each method under the two-wavelength setting.

The corresponding quantitative errors are summarized in Figure 3, which presents both mean absolute error (MAE) in μM and mean relative error (MRE) in % for HbO and Hb. Among the single-distance variants, the 2.5-cm S-D separation produced the lowest MAE (1.89 μM) and MRE

(3.21%) for HbO, while the most accurate Hb estimation occurred at the 2.0-cm S-D separation, with an MAE of 0.34 μM and an MRE of 1.42%. These results indicate that different S-D separations may yield optimal performance for different chromophores; nevertheless, all single-distance implementations at 2.0 – 3.0 cm achieved better accuracy than the slope method for both hemoglobin species. In contrast, the 3.5 cm separation consistently exhibited higher errors in both MAE and MRE, likely due to diminished phase signal quality and increased susceptibility to modeling inaccuracies at extended S-D distances.

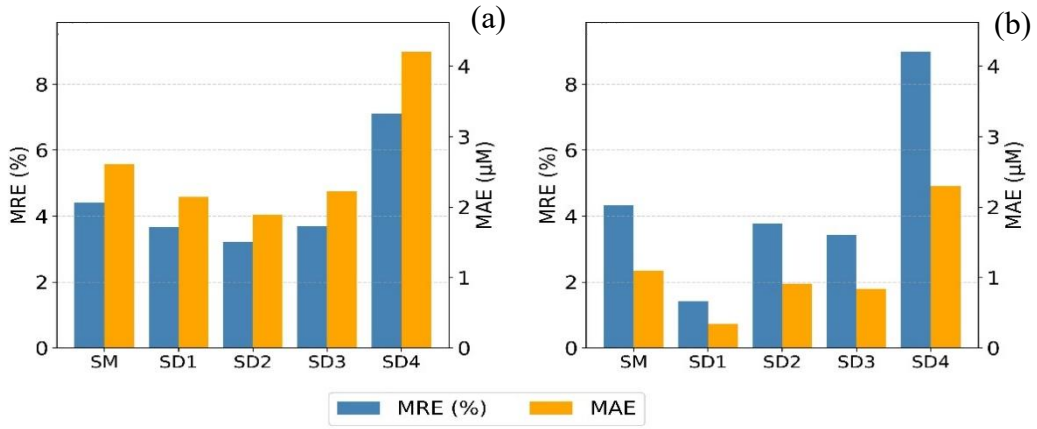

Fig. 3. Error comparison for hemoglobin concentration estimates using the two-wavelength configuration (690 nm and 830 nm). Subplots show mean relative error (MRE, blue bars; left axis) and mean absolute error (MAE, orange bars; right axis) for (a) HbO and (b) Hb across five methods: slope method (SM) and single-distance phase-only inversions at S-D separations of 2.0 cm (SD1), 2.5 cm (SD2), 3.0 cm (SD3), and 3.5 cm (SD4).

In addition to concentration-level validation, we evaluated reconstruction accuracy of the optical properties at each wavelength. Tables 1 and 2 report MRE and MAE values in μ_a and μ_s', respectively, for both wavelengths. The results demonstrate that the reconstructed values using FD_{1SD_phase} are comparable to those using the slope method across most separations, with MRE values being lower than 5%. This reflects the new algorithm's capacity to reliably reconstruct both

light absorption and scattering behavior despite relying solely on single S-D separation and single-phase information.

Table 1: MRE and MAE in μ_a estimates at 690 nm and 830 nm

Wave-length (nm)	Slope Method		SD1 = 2.0 cm		SD2 = 2.5 cm		SD3 = 3.0 cm		SD4 = 3.5 cm	
	MRE (%)	MAE (cm^{-1})	MRE (%)	MAE (cm^{-1})	MRE (%)	MAE (cm^{-1})	MRE (%)	MAE (cm^{-1})	MRE (%)	MAE (cm^{-1})
690	2.31	0.004	1.71	0.003	3.37	0.006	3.05	0.005	5.67	0.01
830	2.33	0.005	2.62	0.005	2.62	0.006	2.81	0.006	4.28	0.009

Table 2: MRE and MAE in μ_s' estimates at 690 nm and 830 nm

Wave-length (nm)	Slope Method		SD1 = 2.0 cm		SD2 = 2.5 cm		SD3 = 3.0 cm		SD4 = 3.5 cm	
	MRE (%)	MAE (cm^{-1})	MRE (%)	MAE (cm^{-1})	MRE (%)	MAE (cm^{-1})	MRE (%)	MAE (cm^{-1})	MRE (%)	MAE (cm^{-1})
690	5.62	0.81	2.83	0.406	2.95	0.424	2.84	0.407	3.30	0.474
830	2.83	0.301	4.80	0.512	4.73	0.504	4.54	0.484	4.74	0.506

4.2. Differential redox-state CCO estimation using eight-wavelength configuration

To evaluate the robustness and spectral generalizability of the proposed inversion framework, we extended the analysis to an eight-wavelength configuration spanning 784–894 nm. This range was selected based on established literature demonstrating its effectiveness for quantifying the differential redox-state concentration of CCO alongside hemoglobin species [9]. The inclusion of CCO_{redox} adds a layer of complexity because of (1) its relatively low concentration in tissue, (2) shallow absorption features, and (3) an increased risk of crosstalk among chromophore estimates.

Similar to the reconstruction procedure used in Section 4.1, estimates of CCO_{redox} across 30 MC simulation samples were obtained using both the slope method (which leverages all separations and paired amplitude-phase data) and the single-distance phase-only algorithm applied

independently at each of the four source-detector separations. The synthetic samples for CCO_{recox} were generated with a mean concentration of 8.5 μM, with a 10% standard deviation.

At its core, our FD_{1SD_phase} algorithm simultaneously estimated five key parameters−HbO, Hb, CCO_{redox}, and the reduced scattering coefficients (a, b)−through direct optimization using all eight-wavelength Monte Carlo simulation results. Notably, this approach bypasses the intermediate step of reconstructing wavelength-specific $\mu_a(\lambda)$ and $\mu_s'(\lambda)$ values. In this way, we significantly simplified the optimization problem by (1) reducing the parameter space dimensionality, (2) eliminating spectral reconstruction-related errors, and (3) improving computational efficiency.

Figure 4 presents a comprehensive comparison between estimated and true concentrations for all three chromophores (HbO, Hb, and CCO_{redox}) across the 30 simulated samples. The proposed FD_{1SD_phase} method demonstrates excellent agreement with ground truth values, particularly at shorter S-D separations (2.0 cm and 2.5 cm). In contrast, the conventional slope method exhibits larger estimation errors, most notably for CCO_{redox}. Key observations include (1) FD_{1SD_phase} maintains strong performance for HbO and Hb up to 3.0 cm separation (Figs. 4(b)-4(d)), and (2) all chromophore estimates show noticeable accuracy degradation at 3.5 cm, as seen in Fig. 4(e). This performance limitation at larger separations primarily may reflect an increased susceptibility to measuring noise and a greater sensitivity to model mismatch errors.

The quantitative errors for the eight-wavelength configuration are summarized in Figure 5, showing both MRE and MAE for HbO, Hb, and CCO_{redox} concentrations. Among the single-distance settings, the 2.0-cm separation yielded the lowest MREs across all three chromophores: 2.95%, 6.71%, and 5.10% for HbO, Hb, and CCO_{redox}, respectively. This separation also achieved the lowest MAEs for HbO (1.68 μM), Hb (1.62 μM), and CCO_{redox} (0.40 μM). These results highlight the robustness of the proposed single-separation, phase-only method in accurately

recovering the CCO_{redox} concentration, which has low-amplitude within the measurement signals. It implies that FD_{1SD_phase} may have minimal sensitivity to scaling effects and measurement noise.

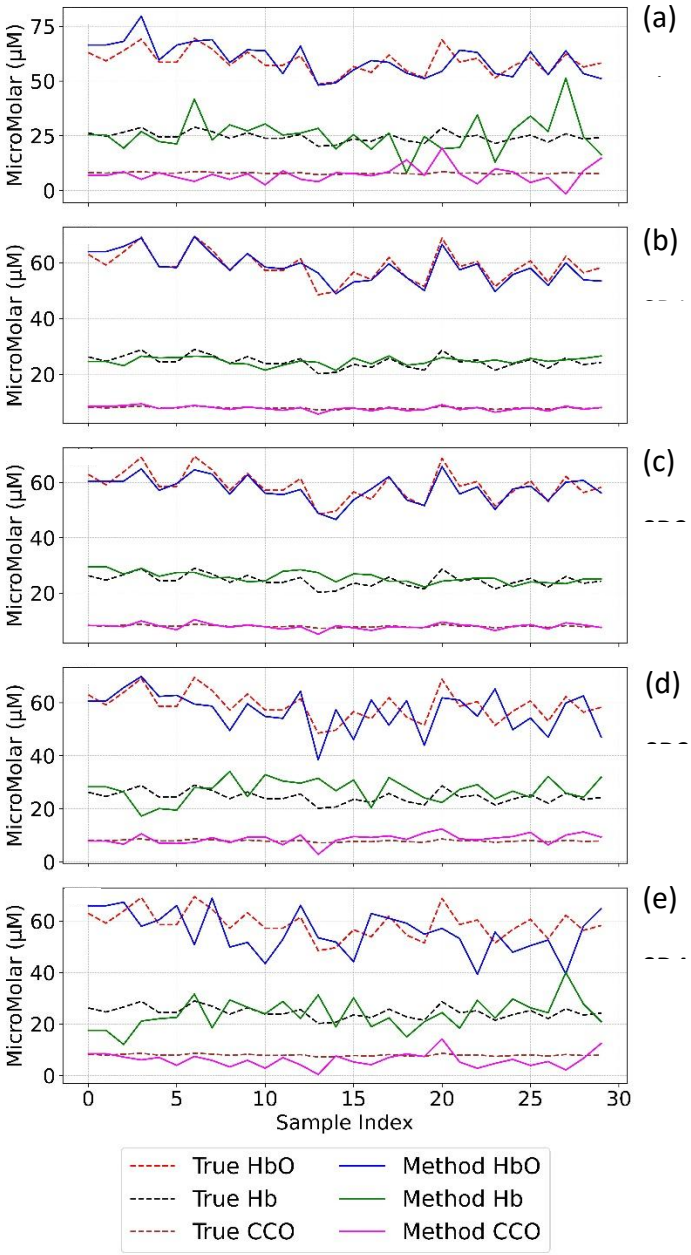

Fig. 4. Comparison of true and estimated concentrations of HbO, Hb, and CCO across 30 synthetic samples using an eight-wavelength FD-NIRS configuration (784, 800, 818, 835, 851, 868, 881, and 894 nm). The reconstructed results were obtained using (a) the conventional slope method and FD_{1SD_phase} at (b) SD1 = 2.0 cm, (c) SD2 = 2.5 cm, (d) SD3 = 3.0 cm, and (e) SD4 = 3.5 cm, respectively. Dashed lines denote ground-truth concentrations, and solid lines represent estimated values.

Figure 5(a) demonstrates that the FD_{1SD_phase} method achieves much lower mean MRE and MAE values at S-D separations equal to or less than 2.5 cm. Moreover, Figs. 5(b)-5(c) reveal that FD_{1SD_phase} consistently outperforms the slope method in both Hb and CCO_{redox} estimation across all separations, with particularly pronounced improvements at 2.0-3.0 cm (SD1-SD3). The most substantial enhancement by our new method was observed for CCO_{redox}, where FD_{1SD_phase} reduced estimation errors remarkably compared to the slope method. The excellence performance of FD_{1SD_phase} remained consistent up to SD2 (S-D separation=2.5 cm), whereas estimations at 3.0 cm and 3.5 cm exhibited a little greater variability and error, likely due to lower phase signal quality and increased sensitivity to model inaccuracies at larger separations. These findings reinforce that the single-separation, phase-only inversion strategy enables high-fidelity quantification of chromophores, including the metabolically critical CCO_{redox}, without reliance on multiple distances or amplitude measurements.

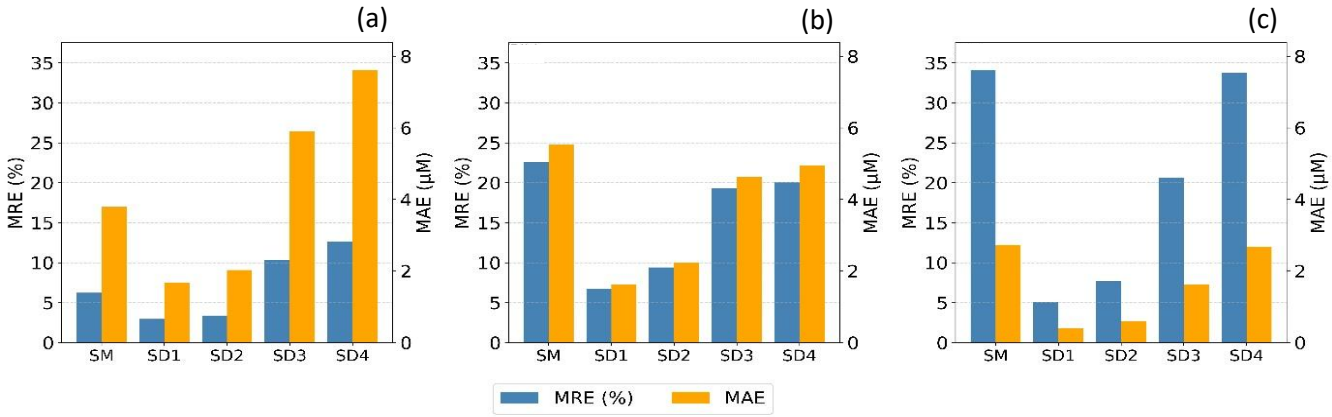

Fig. 5. Error comparison for chromophore concentration estimates using the eight-wavelength configuration. Subplots represent comparative results for (a) HbO, (b) Hb, and (c) CCO_{redox}. Each panel shows MRE (blue bars; left axis) and MAE (orange bars; right axis) for the slope method (SM) and single-distance phase-only inversions at S-D separations of 2.0 cm (SD1), 2.5 cm (SD2), 3.0 cm (SD3), and 3.5 cm (SD4).

To assess the quality of spectral reconstruction beyond chromophore-level summaries, we evaluated wavelength-wise errors in $\mu_a(\lambda)$ and μ_s'. Tables 3 and 4 report MRE and MAE values for both $\mu_a(\lambda)$ and μ_s', respectively, at each individual wavelength for both methods. The results from both tables reaffirm the patterns seen in concentration-level comparisons. The 2.0 and 2.5 cm configurations yield low spectral errors, while MRE and MAE values rise substantially at longer separations (>3 cm). The slope method provides moderate spectral accuracy but is consistently outperformed by the FD_{1SD_phase} algorithm at optimal distances.

Table 3: MRE and MAE in μ_a estimates at each of the eight wavelengths

Wave-length (nm)	Slope Method		SD1 = 2.0 cm		SD2 = 2.5 cm		SD3 = 3.0 cm		SD4 = 3.5 cm	
	MRE (%)	MAE (cm^{-1})	MRE (%)	MAE (cm^{-1})	MRE (%)	MAE (cm^{-1})	MRE (%)	MAE (cm^{-1})	MRE (%)	MAE (cm^{-1})
784	1.63	0.004	1.66	0.004	2.03	0.004	5.79	0.012	8.38	0.019
800	1.84	0.004	1.65	0.004	1.75	0.004	5.28	0.011	8.91	0.02
818	2.36	0.006	1.70	0.004	1.74	0.004	5.27	0.012	9.01	0.022
835	1.92	0.005	1.66	0.004	1.71	0.005	5.14	0.013	8.51	0.023
851	2.24	0.006	1.67	0.005	1.75	0.005	5.19	0.014	8.36	0.024
868	2.20	0.006	1.69	0.005	1.82	0.005	5.24	0.015	8.23	0.024
881	1.67	0.005	1.70	0.005	1.88	0.006	5.26	0.015	8.15	0.024
894	2.09	0.006	1.70	0.005	1.93	0.006	5.29	0.015	8.09	0.025

Table 4: MRE and MAE in μ_s' estimates across all wavelengths.

Wave-length (nm)	Slope Method		SD1 = 2.0 cm		SD2 = 2.5 cm		SD3 = 3.0 cm		SD4 = 3.5 cm	
	MRE (%)	MAE (cm^{-1})	MRE (%)	MAE (cm^{-1})	MRE (%)	MAE (cm^{-1})	MRE (%)	MAE (cm^{-1})	MRE (%)	MAE (cm^{-1})
784	3.51	0.412	3.78	0.441	3.41	0.398	5.63	0.657	5.83	0.683
800	2.62	0.297	3.91	0.442	3.36	0.379	5.57	0.631	5.53	0.627
818	4.60	0.505	3.99	0.436	3.40	0.371	5.85	0.639	5.89	0.645
835	3.87	0.411	4.23	0.447	3.61	0.382	6.04	0.641	5.88	0.622
851	3.13	0.321	4.50	0.461	3.96	0.406	6.48	0.664	6.30	0.645
868	4.20	0.419	4.32	0.43	3.69	0.367	6.42	0.64	6.43	0.643
881	4.57	0.444	4.69	0.455	4.00	0.388	6.75	0.656	6.41	0.625
894	3.81	0.362	4.86	0.46	4.22	0.4	6.95	0.658	7.35	0.699

5 Discussion

5.1 Reconstruction of chromophore concentrations using FD_{1SD_phase}

The results of this study demonstrate that the proposed single-distance, phase-only optimization inversion algorithm for FD-NIRS achieves accurate and robust estimation of chromophore concentrations, outperforming the conventional slope method across multiple evaluation metrics. Across both the two-wavelength and eight-wavelength configurations, our novel method consistently produced lower or comparable mean absolute and relative errors for HbO and Hb concentrations, while uniquely enabling the reliable quantification of differential redox-state concentration of CCO, a chromophore that is notoriously difficult to recover with FD-NIRS.

The excellent performance of FD_{1SD_phase} held across a range of separations, with optimal results typically obtained at or shorter than S-D separations of 2.5 cm. Even when estimation was repeated independently at different separations (SD1–SD4), the algorithm exhibited strong generalizability and multi-separation consistency, with stable performance across varying distances and simulation conditions. These findings suggest that the method is not only accurate but also robust to spatial sampling variation, which is particularly valuable for clinical or wearable FD-NIRS systems with constrained hardware configurations.

Compared to the slope method, which depends on paired AC amplitude and phase measurements across multiple distances, the FD_{1SD_phase} method dramatically reduces system complexity and channel requirements. This simplification could enable broader adoption of FD-NIRS in compact or cost-sensitive platforms. Moreover, while the algorithm is not designed to achieve formal depth resolution, its ability to isolate absorption and scattering effects from a single measurement geometry suggests that FD_{1SD_phase} may be well-suited for integration with

tomographic or multi-layer reconstruction strategies, potentially enabling hybrid depth-sensitive implementations.

To ensure a fair evaluation of the slope method, we also analyzed an alternative configuration using only three source-detector separations, excluding the largest separation (3.5 cm) due to its relatively poor phase quality under high scattering conditions. However, the resulting estimation accuracy showed no meaningful advantage over the standard four-distance configuration (data not shown). In some cases, the error for one wavelength or chromophore slightly improved, but this was offset by worse performance at other wavelengths. This pattern held for both two-wavelength and eight-wavelength cases, reinforcing that removing a noisy channel does not consistently benefit the slope method.

The superior performance of FD_{1SD_phase} stems from its elimination of the intermediate spectral reconstruction step, bypassing the need to calculate wavelength-specific $\mu_a(\lambda)$ and $\mu_s'(\lambda)$ values. This innovative approach achieves significant dimensionality reduction in the optimization problem by directly estimating the five target parameters (HbO, Hb, CCOredox, and scattering coefficients a/b), instead of 16 parameters in the 8-wavelength case, from raw phase data. However, the method's effectiveness is currently limited to hemoglobin-containing tissues or phantoms, as its parameterization specifically accounts for hemoglobin's characteristic absorption features.

5.2 Reconstruction of optical properties using FD_{1SD_phase}

The FD_{1SD_phase} method also achieved strong agreement in the reconstruction of wavelength-resolved optical coefficients (i.e., μ_a and μ_s'), following accurate quantification of hemoglobin-only or multi-chromophore estimations, as outlined in Fig. 1. Estimates of μ_a were consistently accurate across all wavelengths, even in the more challenging broadband case. Reconstructed

values of μ_s' were slightly overestimated across conditions, but the associated errors remained within acceptable bounds. This set of observations indicates that the regularized optimization framework effectively constrained overfitting while preserving spectral detail.

5.3 Key contribution of the developed method, FD_{1SD_phase}

The successful reconstruction of CCO_{redox} concentrations provides strong validation of FD_{1SD_phase}'s methodological advantages. Notably, while the slope method failed to achieve reliable CCO_{redox} estimation (showing >30% relative error) even when using an optimized wavelength set [9], FD_{1SD_phase} reduced this error to <10%. This level of accuracy represents a significant advancement in FD-NIRS quantification, as such precision for CCO_{redox} measurement has rarely been demonstrated by FD-NIRS. These results establish that, with proper modeling, single-distance, phase-only FD-NIRS can reliably quantify mitochondrial metabolism markers without requiring multi-distance or multi-frequency measurements. This breakthrough enables reliable tracking of cellular energy metabolism using practical, single-distance FD-NIRS measurements.

5.4 Limitations of this study

Despite these promising results, several limitations warrant discussion. First, the algorithm is presently constrained to hemoglobin-dominant tissues because it requires hemoglobin's spectral signature for the phase-based optimization. Second, the present study is based exclusively on Monte Carlo simulated data with a limited range of chromophore concentrations. While this provides a rigorous and controllable test environment, experimental validation using actual measurements in tissue-mimicking phantoms or biological tissue will be essential to confirm translational feasibility. Third, the method assumes a homogeneous tissue volume and does not currently account for layered structures or heterogeneous scattering. Last, although the algorithm demonstrated robustness to initialization and noise, further optimization of regularization

strategies may improve performance, particularly for weakly absorbing chromophores or lower signal-to-noise conditions.

6. Conclusion

This work presents a computationally efficient and experimentally scalable framework for quantitative FD-NIRS using single-distance, single-frequency, phase-only measurements. Using Monte Carlo-generated synthetic data, we demonstrate that phase data from a single source-detector pair can enable accurate recovery of both chromophore concentrations and tissue optical properties. Our method significantly outperforms the conventional slope method in hemoglobin-only quantification and multi-chromophore assessment, including the differential redox-state concentration of CCO, a long-standing challenge in FD-based systems. The algorithm's success stems from its innovative dimensionality reduction approach, which directly estimates chromophore concentrations while bypassing intermediate spectral reconstruction steps. Although currently validated through in silico studies, the results demonstrate the robustness against measurement noise and the scalability to diverse chromophore targets, leading to strong potential for clinical translations.

Future efforts include experimental validation, extension to heterogeneous or layered tissues, and integration with tomographic frameworks to enable depth-sensitive analysis. Collectively, this study establishes a new paradigm for developing simplified yet spectrally comprehensive FD-NIRS systems capable of absolute quantification of both vascular (HbO/Hb) and metabolic (CCOredox) markers.

Disclosures

The authors declare no conflicts of interest. No relevant financial interests in the manuscript and no other potential conflicts of interest to disclose.

Code, Data, and Materials

The data presented in this study are available on request from the corresponding author.

Acknowledgments

This research was funded in part by the NIA (R21AG079309) of the National Institutes of Health.

References:

[1] J. B. Fishkin and E. Gratton, "Propagation of photon-density waves in strongly scattering media containing an absorbing semi-infinite plane bounded by a straight edge," *J Opt Soc Am A,* vol. 10, no. 1, pp. 127-40, Jan 1993, doi: 10.1364/josaa.10.000127.

[2] S. Fantini, M. A. Franceschini, J. B. Fishkin, B. Barbieri, and E. Gratton, "Quantitative determination of the absorption spectra of chromophores in strongly scattering media: a light-emitting-diode based technique," *Appl Opt,* vol. 33, no. 22, pp. 5204-13, Aug 1 1994, doi: 10.1364/AO.33.005204.

[3] I. Bigio, J. and S. Fantini, *Quantitative Biomedical Optics: Theory, Methods, and Applications*. Cambridge University Press, 2016.

[4] C. Kolyva *et al.*, "Systematic investigation of changes in oxidized cerebral cytochrome c oxidase concentration during frontal lobe activation in healthy adults," *Biomed Opt Express,* vol. 3, no. 10, pp. 2550-66, Oct 1 2012, doi: 10.1364/BOE.3.002550.

[5] D. M. Hueber *et al.*, "Non-invasive and quantitative near-infrared haemoglobin spectrometry in the piglet brain during hypoxic stress, using a frequency-domain multidistance instrument," *Phys. Med. Biol.,* vol. 46, pp. 41–62, 2001.

[6] B. J. Tromberg *et al.*, "Non-invasive measurements of breast tissue optical properties using frequency-domain photon migration," *Philos Trans R Soc Lond B Biol Sci,* vol. 352, no. 1354, pp. 661-8, Jun 29 1997, doi: 10.1098/rstb.1997.0047.

[7] A. Sassaroli, G. Blaney, and S. Fantini, "Dual-slope method for enhanced depth sensitivity in diffuse optical spectroscopy," *Journal of the Optical Society of America A,* vol. 36, no. 10, pp. 1743-1761, 2019.

[8] S. Fantini and A. Sassarol, "Frequency-Domain Techniques for Cerebral and Functional Near-Infrared Spectroscopy," *Front. Neurosci.,* vol. 14, 2020.

[9] D. Arifler, T. Zhu, S. Madaan, and I. Tachtsidis, "Optimal wavelength combinations for near-infrared spectroscopic monitoring of changes in brain tissue hemoglobin and cytochrome c oxidase concentrations," *Biomed Opt Express,* vol. 6, no. 3, pp. 933-47, Mar 1 2015, doi: 10.1364/BOE.6.000933.

[10] G. Bale, C. E. Elwell, and I. Tachtsidis, "From Jobsis to the present day: a review of clinical near-infrared spectroscopy measurements of cerebral cytochrome-c-oxidase," *J Biomed Opt,* vol. 21, no. 9, p. 091307, Sep 2016, doi: 10.1117/1.JBO.21.9.091307.

[11] G. Leadley, T. Austin, and G. Bale, "Review of measurements and imaging of cytochrome-c-oxidase in humans using near-infrared spectroscopy: an update," *Biomed Opt Express,* vol. 15, no. 1, pp. 162-184, Jan 1 2024, doi: 10.1364/BOE.501915.

[12] H. Z. Yeganeh, V. Toronov, J. T. Elliott, M. Diop, T. Y. Lee, and K. St Lawrence, "Broadband continuous-wave technique to measure baseline values and changes in the tissue chromophore concentrations," *Biomed Opt Express,* vol. 3, no. 11, pp. 2761-70, Nov 1 2012, doi: 10.1364/BOE.3.002761.

[13] S. L. Jacques, "Optical properties of biological tissues: a review," *Phys Med Biol,* vol. 58, no. 11, pp. R37-61, Jun 7 2013, doi: 10.1088/0031-9155/58/11/R37.

[14] R. H. Byrd , P. Lu , J. Nocedal , and C. Zhu "A Limited Memory Algorithm for Bound Constrained Optimization ", ed, 1995.

[15] S. Yan and Q. Fang, "Hybrid mesh and voxel based Monte Carlo algorithm for accurate and efficient photon transport modeling in complex bio-tissues," (in eng), *Biomed Opt Express,* vol. 11, no. 11, pp. 6262-6270, Nov 01 2020, doi: 10.1364/BOE.409468.

Figure Captions

Fig. 1 Flowchart to present the simulation and analysis workflow used in this study. It starts from a chosen set of chromophore concentrations (HbO and Hb with or without CCO_{redox}), followed by corresponding $\mu_a(\lambda)$ for given wavelengths (either 2 or 8 wavelengths). Then, FD-NIRS parameters (i.e., DC, AC, and phase values) were extracted from the time-domain MC simulations after the Fourier transform. Next, both the slope method and single S-D, phase-only optimization method were used to reconstruct chromophore concentrations.

Fig. 2 Comparison of true and estimated concentrations of HbO and Hb across 30 synthetic samples using a two-wavelength FD-NIRS configuration (690 nm and 830 nm). The reconstructed results were obtained using (a) the conventional slope method and FD_{1SD_phase} at (b) SD1 = 2.0 cm, (c) SD2 = 2.5 cm, (d) SD3 = 3.0 cm, and (e) SD4 = 3.5 cm, respectively. Dashed lines represent ground-truth concentrations, while solid lines denote model estimates. The agreement across samples highlights the performance of each method under the two-wavelength setting.

Fig. 3 Error comparison for hemoglobin concentration estimates using the two-wavelength configuration (690 nm and 830 nm). Subplots show mean relative error (MRE, blue bars; left axis) and mean absolute error (MAE, orange bars; right axis) for (a) HbO and (b) Hb across five methods: slope method (SM) and single-distance phase-only inversions at S-D separations of 2.0 cm (SD1), 2.5 cm (SD2), 3.0 cm (SD3), and 3.5 cm (SD4).

Fig. 4 Comparison of true and estimated concentrations of HbO, Hb, and CCO across 30 synthetic samples using an eight-wavelength FD-NIRS configuration (784, 800, 818, 835, 851, 868, 881, and 894 nm). The reconstructed results were obtained using (a) the conventional slope method and FD_{1SD_phase} at (b) SD1 = 2.0 cm, (c) SD2 = 2.5 cm, (d) SD3 = 3.0 cm, and (e) SD4 = 3.5 cm, respectively. Dashed lines denote ground-truth concentrations, and solid lines represent estimated values.

Fig. 5 Error comparison for chromophore concentration estimates using the eight-wavelength configuration. Subplots represent comparative results for (a) HbO, (b) Hb, and (c) CCO_{redox}. Each panel shows MRE (blue bars; left axis) and MAE (orange bars; right axis) for the slope method (SM) and single-distance phase-only inversions at S-D separations of 2.0 cm (SD1), 2.5 cm (SD2), 3.0 cm (SD3), and 3.5 cm (SD4).